Supplementary Material

Salt Contribution to RNA tertiary structure folding stability

Zhi-Jie TAN[1] and Shi-Jie CHEN[2]

[1]Department of Physics and Key Laboratory of Artificial Micro & Nano-structures of Ministry of Education, School of Physics and Technology, Wuhan University, Wuhan, P.R. China 430072

[2]Department of Physics and Astronomy and Department of Biochemistry, University of Missouri, Columbia, MO 65211

Framework of Tightly bound ion model

The high concentration of counterions near RNA surface could potentially cause strong correlation (coupling) between the ions. Such an effect is stronger for multivalent ions. To account for this potentially important effect, we classify the multivalent ions into two types (1)-(7): the (strongly correlated) tightly bound (TB) ions and the (weakly correlated) diffusively bound ions. The corresponding spatial regions are called the TB region and the diffusive region, respectively. It is important to note that the TB ions are mobile and involve no site-specific binding. For the TB ions, we enumerate discrete ion distributions to account for the correlation effect. For the diffusively bound ions, we use the mean-field (Poisson-Boltzmann) equation. We treat the monovalent ions, whose correlation effect is negligible, as diffusive ionic background.

To enumerate the ion distributions for the TB ions, we discretize the TB region into cells, each around a phosphate, and describe the ion distribution (also called ion binding mode) in a coarse-grained representation (as the number of ions in each cell). The total partition function Z for the TB ions is given by the summation over all the possible binding modes M : $Z = \sum_M Z_M$, where Z_M is the partition function for a binding mode M. The electrostatic free energy for a given RNA structure is determined as $G^E = -k_BT \ln \sum_M (Z_M)$. The details about the numerical computation and the parameter sets are described in the Supplementary Material. As illustrated in Fig. S6, because the correlation effect causes the TB ions to self-organize and form the low-energy states that cannot be reached by the mean-field states, the TBI model may give improved predictions for RNA-Mg^{2+} interactions (7).

Tightly bound ion model for atomic RNA structure

The original TBI model (1–5) based on the coarse-grained nucleic acid structural model (6) has been refined to treat atomic nucleic acid structures (7). Here, we only introduce the model briefly; see Ref. (7) for details.

In the model, the multivalent (z) ions are classified into two types according to the ion-ion correlation (1)-(7): the (strongly correlated) tightly bound ions and the (weakly correlated) diffusively bound ions, and correspondingly, the regions where the two types of ions reside are denoted as tightly bound region and diffusive region, respectively. The motivation to distinguish these two types of z-valent ions (and the two types of spatial regions for z-valent ions) is to treat them separately: for the diffusive ions, we use mean-field (PB) approach; for the tightly bound ions, we use a separate treatment that can account for the strong ion-ion correlations and ion-binding ensemble. Simultaneously, the monovalent ions are treated as diffusive ionic background with the mean-field approach due to the weak inter-ion Coulombic correlations.

For a N-nt RNA molecule, the whole tightly bound region is divided into N cells, each around a phosphate. For the RNA, there exist a large number of binding modes for different ions binding in different cells, and the total partition function Z is given by the summation over all the possible binding modes M:

$$Z = \sum_M Z_M. \tag{1}$$

Z_M is the partition function for a given binding mode M (1)-(7)

$$Z_M = Z^{(id)} \left(\frac{N_z}{V}\right)^{N_b} \left(\int \prod_{i=1}^{N_b} d\mathbf{R}_i\right) e^{-(\Delta G_b + \Delta G_d + \Delta G_b^{pol})/k_B T} \quad (2)$$

where $Z^{(id)}$ is the partition function for the uniform ion solution (without the polyelectrolyte). N_z is the total number of z-valent counterions and V is the volume of the solution. N_b and $\int \prod_{i=1}^{N_b} d\mathbf{R}_i$ are the number and the volume integral for the tightly bound ions, respectively. ΔG_b is the mean Coulombic interaction energy between all the discrete charge-charge pairs (including the phosphate groups and the tightly bound ions) in the tightly bound region; ΔG_d is the free energy for the electrostatic interactions between the diffusive ions and between the diffusive ions and the discrete charges in the tightly bound region, and the entropic free energy of the diffusive ions. ΔG_b^{pol} is the (Born) self-polarization energy for the discrete charges in the tightly bound region (4, 7). ΔG_b, ΔG_d, and ΔG_b^{pol} have been given in detail in Refs (1)-(7).

Therefore, the electrostatic free energy for a RNA molecule can be computed by

$$G^E = -k_B T \ln \sum_M \left(Z_M / Z^{(id)}\right). \quad (3)$$

The numerical computation and parameter sets are described briefly in the following; see Ref. (4, 7) for details.

Computations and parameter sets

The computation of the TBI model is divided into three steps (1)-(7): (*i*) First, we solve the PB equation for an atomic RNA molecule in salt solution, to obtain the $z-$valent ion distributions, from which we determine the tightly bound region for $z-$valent ions (1)-(7). Here, the atomic RNA is defined by the sum of the van der Waals radii of all the atoms in the RNA (http://www.rbvi.ucsf.edu/chimera/docs/UsersGuide/midas/vdwtables.html). (*ii*) Second, we compute the pair-wise potentials of mean force $\Phi_1(i)$ and $\Phi_2(i, j)$ and Born energy $\Phi_0(i)$, with the use of the general Born model (4, 5, 7). The exclusions between ions and nucleic acid atoms are accounted for by a truncated Lenard-Jones potential: $U = u_0(\frac{1}{r^{12}} - \frac{1}{r^6})$ for $r < 1$ and $U = 0$ for $r > 1$, where r is the distance between an ion and an atom in the unit of the sum of the radii for the ion and atom (7). Here, u_0 is taken as 0.35 due to the soft H-atom exclusion (7, 8). The calculated $\Phi_1(i)$ and $\Phi_2(i, j)$ and $\Phi_0(i)$ are tabulated and stored for the following calculations of partition function. (*iii*) Third, we enumerate the possible binding modes. For each mode, we calculate ΔG_b, ΔG_d, and ΔG_b^{pol} (4, 5, 7). Summation over the binding modes gives the total partition function Z (Eq. 1), from which we can calculate the electrostatic free energy for a RNA molecule. For long molecules, we have previously proposed a framework by separately treating high-energy modes and low-energy modes (2).

In this work, ions are assumed to be hydrated (1)-(4), and have the radii: Na^+, 3.5 Å; and Mg^{2+}, 4.5 Å (1)-(7, 9), respectively. Here, the dielectric constant ϵ of nucleic acid interior is set to be 20 (4, 7), and the molecule exterior is taken as that of water (10)

$$\epsilon(t) = 87.740 - 0.4008 \times t + 9.398 \times 10^{-4} \times t^2 - 1.41 \times 10^{-6} \times t^3, \quad (4)$$

where t is the solution temperature in Celsius. When solving PB equation, a thin layer of thickness of a cation radius is added to the molecular surface to account for the excluded volume layer of the cations (1)-(7), and the three-step focusing process is used to obtain the detailed ion distribution near RNA molecules (1)-(7, 11). For each run, the electrostatic potentials are iterated to a convergence of $< 10^{-4} k_B T/q$. The resolution of the first run varies with the grid size to make the iterative process doable (1)-(7), and the resolutions for the second and third runs are 1.36 Å per grid and 0.68 Å per grid, respectively. Our results are stable as tested against different grid sizes.

Parameterizations for the salt contributions to RNA tertiary structure folding

In the main text, we showed that our predictions for the Mg^{2+} contribution ($\Delta\Delta g_{Mg^{2+}}$) to RNA tertiary structure folding agree well with the available experimental data. Similar to the empirical formulas for DNA and RNA helices in various $Na^+(K^+)/Mg^{2+}$ solutions, we fit empirical formulas for the electrostatic free energy for the different RNA structures in terms of the compactness of the RNA structure and the logarithms of the cation concentrations (12–16). Based on the systematic calculations for six RNAs (BWYV pseudoknot, MMTV pseudoknot, T2 pseudoknot, kissing complex, 58-nt rRNA fragment, and yeast $tRNA^{Phe}$), we fit an empirical formula for ΔG^E as a function of $[Na^+]$, $[Mg^{2+}]$, and sequence length and the compactness ($r_g = R_g^0/R_g$) of the structure.

In a Na^+ solution.

Based on the systematic calculations for the different RNAs, we fit the following empirical formula for the electrostatic free energy ΔG^E (in kcal/mol) for RNA tertiary structure folding in pure Na^+ solutions

$$\Delta G^E[Na^+] = \Delta G^E_{1M\,Na^+} + a_1 N \ln[Na^+] + b_1 N \ln^2[Na^+], \tag{5}$$

where $\Delta G_{1M\,Na^+}$ (in kcal/mol) is the folding free energy at standard 1M Na^+ salt and $r_g(=R_g^0/R_g)$ quantifies the folding compactness; see Table I. The coefficients a_1 and b_1 are given by

$$\begin{aligned} a_1 \times \epsilon^*(T)T^* &= -0.086 + 7/(Nr_g^3 + 65); \\ b_1 \times \epsilon^*(T)T^* &= 0.008 - 3.6/(N-5)^2, \end{aligned} \tag{6}$$

where $\epsilon^*(T)(= \frac{\epsilon(T)}{\epsilon(298.15\,K)})$ is the relative dielectric constant of the solvent at absolute temperature T (with respect to the room temperature), as given by in Supplementary Material. $T^*(= \frac{T}{298.15})$ is the relative absolute temperature with respect to the room temperature. As shown in Fig. S7 in Supplementary Material, Eq. 5 gives good fit to the calculated electrostatic folding free energies in pure Na^+ solutions for the six RNAs at the different temperatures.

In a Mg^{2+} solution.

For the tertiary structure folding in pure Mg^{2+}, we have the following empirical formula for the electrostatic folding free energy

$$\Delta G^E[Mg^{2+}] = \Delta G^E_{1M\,Na^+} + a_2 N \ln[Mg^{2+}] + b_2 N \ln^2[Mg^{2+}] + c_2 N T^*, \tag{7}$$

where the coefficients a_2, b_2, and c_2 are given respectively by

$$\begin{aligned} a_2 \times \epsilon^*(T)T^* &= 0.012 - 1.4/(Nr_g^3 + 75); \\ b_2 \times \epsilon^*(T)T^* &= 0.0048 - 57/(Nr_g^3 + N + 75)(N + 75); \\ c_2 \times \epsilon^*(T)T^* &= -0.27 + 0.16/r_g^3 + 1.4/N. \end{aligned} \tag{8}$$

Fig. S8 (in Supplementary Material) shows that Eq. 7 fits the calculated electrostatic folding free energy very well, for the six studied RNAs in pure Mg^{2+} solutions.

In a mixed Na^+/Mg^{2+} solution.

For mixed Na^+/Mg^{2+} solutions, we fit the following empirical formula for the electrostatic folding free energy $\Delta G[Na^+/Mg^{2+}]$:

$$\Delta G^E[Na^+/Mg^{2+}] = x\Delta G^E[Na^+] + (1-x)\Delta G^E[Mg^{2+}] + N\Delta g_{12}, \tag{9}$$

where the first two terms represent the fractional contributions from Na^+ and Mg^{2+} respectively, and x is given by

$$x = \frac{[Na^+]}{[Na^+] + (3.8 - 34/(N-20)r_g^3)(1 + 0.2[Na^+])[Mg^{2+}]^{0.64}}. \tag{10}$$

The third term in Eq. 9 gives the cross-term for the Na^+-Mg^{2+} interference, and Δg_{12} is given by

$$\Delta g_{12} = -x(1-x)(0.26 - 1.2/(N-20)), \tag{11}$$

As shown in Fig. S9 (in Supplementary Material), Eq. 9 gives good fit with the TBI calculations on $\Delta G^E[Na^+/Mg^{2+}]$.

Mg^{2+}-contribution to RNA tertiary structure folding.

As shown in Fig. S10, for BWYV pseudoknot, 58-nt rRNA fragment, and yeast $tRNA^{Phe}$, the empirical formulas (Eqs. 5-9) give good predictions on the Mg^{2+}-contributions $\Delta\Delta G_{Mg^{2+}}$ to RNA tertiary folding free energy, as compared with the experimental data (17, 19–21).

K^+/Mg^{2+}-dependent RNA tertiary stability

The above experimental comparisons show that the empirical formulas can give good predictions on RNA folding free energy in Na^+ and mixed Na^+/Mg^{2+} solutions. Our previous studies shows that for RNA secondary segments (e.g. helix and hairpin), the empirical formulas derived from the ionic conditions of mixed Na^+/Mg^{2+} can also be used to predicted the case of mixed K^+/Mg^{2+} (14, 15). In this section, we will also use the empirical formulas derived from Na^+/Mg^{2+} solutions to predict the RNA tertiary folding stability in K^+ and mixed K^+/Mg^{2+} solutions, and compared the predictions with the available experimental data.

MMTV pseudoknot

Fig. S11(A) shows the melting temperature T_m for MMTV pseudoknot as a function of $[K^+]$. The experimental comparisons show that our predicted T_m with the formula for Na^+ is slightly higher than that for K^+, suggesting slightly stronger tertiary stabilization role of Na^+ than K^+. This finding is also in accordance with the other experimental findings on ion-binding affinity (22) and on RNA tertiary folding (23), where Na^+ has (slightly) higher binding affinity (22) and is (slightly) more efficient in inducing RNA tertiary folding than K^+ (23).

Fig. S11(B) shows the predicted T_m of MMTV pseudoknot in mixed K^+/Mg^{2+} solutions. Our predicted T_m's agree well with the experimental data for high $[Mg^{2+}]$, while are slightly higher than the measured values for low $[Mg^{2+}]$ (24); see the curve for 50mM K^+. These phenomena may come from the different roles of Na^+ and K^+. At high $[Mg^{2+}]$, Mg^{2+} dominates system, and the predictions are close to the experimental data. But for low $[Mg^{2+}]$ where K^+ dominates the folding stability, our predictions with the formulas for Na^+ slightly overestimate the folding stability, which corresponds to the slightly weaker role of K^+ (than Na^+) in RNA tertiary stabilization.

T2 pseudoknot

The thermodynamic experiment indicates that the tertiary folding of T2 pseudoknot exhibits two sub-transitions from the secondary intermediate state to the native state (25). We can estimate the tertiary folding free energy for the T2 pseudoknot.

Fig. S11(C) shows the folding free energy ΔG as a function of $[K^+]$. Our prediction with the formulas for Na^+ slightly underestimates the K^+-concentration dependence of ΔG, i.e., ΔG has slightly stronger ion-concentration dependence in K^+ than in Na^+. This may come from the slightly weaker K^+-binding affinity to nucleic acids (than Na^+) (22). Thus K^+-binding is (slightly) less enthalpically favorable and more entropically favorable than Na^+. Therefore, ion-concentration has stronger influence on K^+-binding than Na^+, causing (slightly) stronger $[K^+]$-dependent stability for RNA tertiary folding.

Fig. S11(D) shows the folding free energy ΔG in mixed K^+/Mg^{2+} solutions. The experimental comparison shows that our predictions with the formulas for Na^+ slightly over-estimate ΔG at high $[Mg^{2+}]$; see the curve for 0.1M K^+ (25). This is also comes from the (slightly) weaker K^+-binding affinity (than Na^+) (22). Consequently, our predictions

with the formulas for Na^+ would slightly overestimate the role of K^+, and simultaneously underestimate the role of Mg^{2+} because the roles of Na^+ (or K^+) and Mg^{2+} are anti-cooperative (7). As the result, the predictions may slightly overestimate ΔG and hence slightly underestimate the tertiary folding stability at high [Mg^{2+}].

Effect of the structural model for the intermediate states

In the present model, following the previous approach (18, 19), we model the average electrostatic properties of intermediate state through an A-form helix with N_0 = 24-nt (see Methods). In order to examine the sensitivity of the predictions on the structural model of the intermediate state, we perform calculations using the different lengths of the A-form helix (N_0=22-nt, and 26-nt, respectively) for the intermediate state.

As shown in Fig. S12, we find that the predictions are not very sensitive to the selected A-form helix length N_0 (around 24-nt) for the intermediate state. The increase of the A-form helix length N_0 only slightly weakens the ion-concentration dependence of electrostatic free energy. For example, when N_0 is increased from 24-nt to 26-nt, for $tRNA^{Phe}$, Δg^E would decrease by $\lesssim$5% at 1M Na^+ and by $\lesssim$6% at 10mM Na^+. For Mg^{2+}, such a decrease in Δg^E would be $\lesssim$5% at 10mM Mg^{2+} and $\lesssim$7% at 0.01mM Mg^{2+}, respectively. Correspondingly, the Mg^{2+}-contribution $\Delta\Delta g_{Mg^{2+}}$ also decreases very slightly, and the maximum decrease occurs at high [Mg^{2+}] when Mg^{2+} accumulation around RNA is the strongest. For $tRNA^{Phe}$ in a Mg^{2+} solution with mixed 32mM Na^+, $\Delta\Delta g_{Mg^{2+}}$ increases by $\sim$7% for 100mM Mg^{2+} when N_0 is increased from 24-nt to 26-nt. For lower [Mg^{2+}] (than 100mM), the decrease in $\Delta\Delta g_{Mg^{2+}}$ is even smaller. Furthermore, as shown in Fig. S12(C), the slight change of N_0 does not affect the good agreements between the predictions and the experimental data for $\Delta\Delta g_{Mg^{2+}}$ (17, 18, 20, 21). From the above control tests, we find that the theoretical predictions are not very sensitive to the selected helix length N_0 around 24-nt for the intermediate state.

Nevertheless, the above model for the intermediate state is a simplified approximation. The realistic intermediate state should be represented as an ensemble of fluctuating conformations whose distribution is dependent on the ionic environment. Although the approximation can give useful results in the present and previous studies, a rigorous thorough study based explicitly on the complete conformational ensemble is needed in order to examine the validity of this simplified model. For example, would the approximation be more reliable for low or high ion concentrations? How is the ion condition coupled to the conformational ensemble heterogeneity and conformational entropy of the intermediate states? Neglecting the conformational ensemble for the intermediate state may cause the underestimation in the conformational entropy of RNA, which could play an important role at high ion concentration and high temperature, and may be responsible for the (slight) overestimation on T_m at very high [Mg^{2+}]. The current form of the model, however, cannot provide such a complete investigation because it would computationally highly demanding to run the TBI computation for each and every conformation in the ensemble.

References

[1] Tan, Z.J., and S.J. Chen. 2005. Electrostatic correlations and fluctuations for ion binding to a finite length polyelectrolyte. *J. Chem. Phys.* 122:044903.

[2] Tan, Z.J., and S.J. Chen. 2006. Ion-mediated nucleic acid helix-helix interactions. *Biophys. J.* 91:518-536.

[3] Tan, Z.J., and S.J. Chen. 2006. Electrostatic free energy landscape for nucleic acid helix assembly. *Nucleic Acids Res.*, 34:6629-6639.

[4] Tan, Z.J., and S.J. Chen. 2008. Electrostatic free energy landscapes for DNA helix bending. *Biophys. J.* 94:3137-3149.

[5] Tan, Z.J. and S.J. Chen. 2009. Predicting electrostatic forces in RNA folding. *Methods Enzymol.* 469:465-487.

[6] Montoro, J.C.G., and J.L.F. Abascal. 1995. Ionic distribution around simple DNA models. I. Cylindrically averaged properties. *J. Chem. Phys.* 103:8273-8284.

[7] Tan, Z.J., and S.J. Chen. 2010. Predicting ion binding properties for RNA tertiary structures. *Biophys. J.* 99: 1565-1576.

[8] Cheatham III, T.E., and M.A. Young. 2001. Molecular dynamics simulation of nucleic acids: Successes, limitations and promise. *Biopolymers* 56:232-256.

[9] Marcus, Y. 1985. Ion Solvation. John Wiley & Sons Ltd., Great Britain.

[10] Eisenberg, D., and W. Kauzmann. 1969. The Structure and Properties of Water. Oxford University Press, Oxford.

[11] Gilson, M.K., K.A. Sharp, and B. Honig. 1987. Calculating the electrostatic potential of molecules in solution: method and error assessment. *J. Comput. Chem.* 9:327-335.

[12] SantaLucia, J.,Jr. 1998. A unified view of polymer, dumbbell, and oligonucleotide DNA nearest-neighbor thermodynamics. *Proc. Natl. Acad. Sci. USA* 95:1460-1465.

[13] Owczarzy, R., Y. You, B.G. Moreira, J.A. Manthey, L. Huang, M. A. Behlke, and J. A. Walder. 2004. Effects of sodium ions on DNA duplex oligomers: improved predictions of melting temperatures. *Biochemistry* 43:3537-3554.

[14] Tan, Z.J., and S.J. Chen. 2008. Salt dependence of nucleic acid hairpin stability. *Biophys. J.* 95:738-752.

[15] Tan, Z.J., and S.J. Chen. 2007. RNA helix stability in mixed Na^+/Mg^{2+} solution. *Biophys. J.* 92:3615-3632.

[16] Tan, Z.J., and S.J. Chen. 2006. Nucleic acid helix stability: effects of salt concentration, cation valency and size, and chain length. *Biophys. J.* 90:1175-1190.

[17] Soto, A.M., V. Misra, and D.E. Draper. 2007. Tertiary structure of an RNA pseudoknot is stabilized by ”diffuse” Mg(2+) ions. *Biochemistry* 46:2973-2983.

[18] Misra, V.K., and D.E. Draper. 2002. The linkage between magnesium binding and RNA folding. *J. Mol. Biol.* 317:507-521.

[19] Misra, V.K., R. Shiman, and D.E. Draper. 2003. A thermodynamic framework for the magnesium-dependent folding of RNA. *Biopolymers* 69:118-136.

[20] Bukhman, Y.V., and D.E. Draper. 1997. Affinities and selectivities of divalent cation binding sites within an RNA tertiary structure. *J. Mol. Biol.* 273:1020-31.

[21] Romer, R., and R. Hach. 1975. tRNA conformation and magnesium binding. A study of a yeast phenylalanine-specific tRNA by a fluorescent indicator and differential melting curves. *Eur. J. Biochem.* 55:271-284.

[22] Bai, Y., M. Greenfeld, K.J. Travers, V.B. Chu, J. Lipfert, S. Doniach, and D. Herschlag. 2007. Quantitative and comprehensive decomposition of the ion atmosphere around nucleic Acids. *J. Am. Chem. Soc.* 129:14981-14988.

[23] Heilman-Miller, S.L., D. Thirumalai, and S.A. Woodson. 2001. Role of counterion condensation in folding of the Tetrahymena ribozyme. I. equilibrium stabilization by cations. *J. Mol. Biol.* 306:1157-1166.

[24] Theimer, C.A., and D.P. Giedroc. 2000. Contribution of the intercalated adenosine at the helical junction to the stability of the gag-pro frameshifting pseudoknot from mouse mammary tumor virus. *RNA* 6:409-21.

[25] Nixon, P.L., and D.P. Giedroc. 1998. Equilibrium unfolding (folding) pathway of a model H-type pseudoknotted RNA: the role of magnesium ions in stability. *Biochemistry* 37:16116-29.

[26] Su, L., L. Chen, M. Egli, J.M. Berger, and A. Rich. 1999. Minor groove RNA triplex in the crystal structure of a ribosomal frameshifting viral pseudoknot. *Nature Struct. Biol.* 6:285-292.

[27] Conn, G.L., A.G. Gittis, E.E. Lattman, V.K. Misra, and D.E. Draper. 2002. A compact RNA tertiary structure contains a buried backbone-K+ complex. *J. Mol. Biol.* 318:963-73.

[28] Westhof, E., and M. Sundaralingam. 1986. Restrained refinement of the monoclinic form of yeast phenylalanine transfer RNA. Temperature factors and dynamics, coordinated waters, and base-pair propeller twist angles. *Biochemistry* 25:4868-4878.

[29] Ennifar, E, P. Walter, B. Ehresmann, C. Ehresmann, and P. Dumas. 2001. Crystal structures of coaxially stacked kissing complexes of the HIV-1 RNA dimerization initiation site. *Nature Struct. Biol.* 8:1064-1068.

[30] Holland, J.A., M.R. Hansen, Z. Du, and D.W. Hoffman. 1999. An examination of coaxial stacking of helical stems in a pseudoknot motif: the gene 32 messenger RNA pseudoknot of bacteriophage T2. *RNA* 5:257-71.

[31] Shen, L.X., and I. Tinoco Jr. 1995. The structure of an RNA pseudoknot that causes efficient frameshifting in mouse mammary tumor virus. *J. Mol. Biol.* 247:963-78

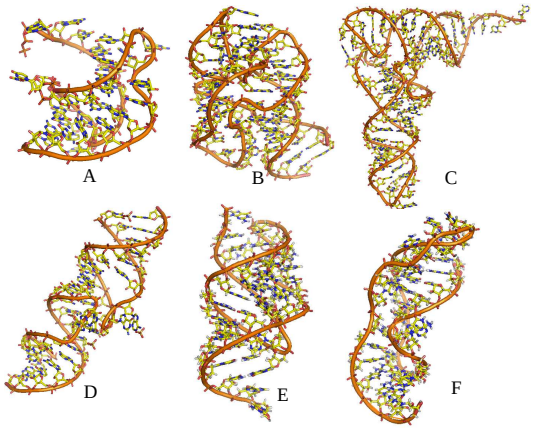

FIGURE S5 (A-F) Illustrations for the 3-dimensional atomic RNA structures: A, BWYV (beet western yellow virus) pseudoknot (PDB code: 437D) (26); B, a 58-nt ribosomal RNA (rRNA) fragment (PDB code: 1HC8) (27); C, yeast $tRNA^{Phe}$ (PDB code: 1TRA) (28); D, HIV-1 $_{Lai}$ DIS kissing complex (PDB code: 2B8S) (29); E, T2 gene 32 mRNA (T2) pseudoknot (PDB code: 2TPK) (30); and F, mouse mammary tumor virus frameshifting (MMTV) pseudoknot (PDB code: 1RNK) (31); see also Table I.

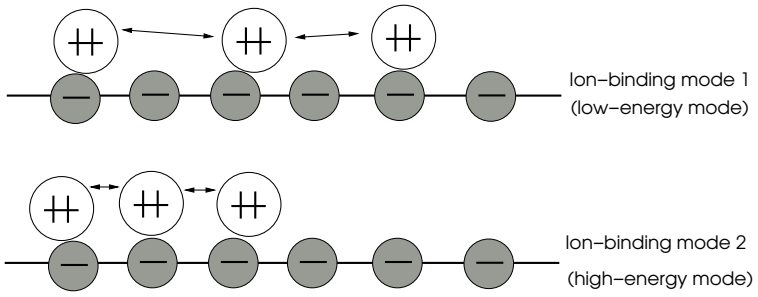

FIGURE S6 A cartoon shows the ion correlations and binding fluctuations/ensemble (modes) are important for multivalent ion binding to a nucleic acid. Mode 1 and mode 2 are with the same numbers of binding ions and the total charges (phosphate charges and ion charges) are neutral. However, the electrostatic energies of the two modes are totally different. The ion-ion correlations and ion-binding ensemble are explicitly accounted in the TBI model, thus the TBI model allows ions, especially multivalent ions to form correlated distributions with much lower energy than a mean-field fluid-like ion distribution can reach, and consequently can make improved predictions on Mg^{2+}-binding. A similar cartoon was shown in Fig. 1 in Ref. (5).

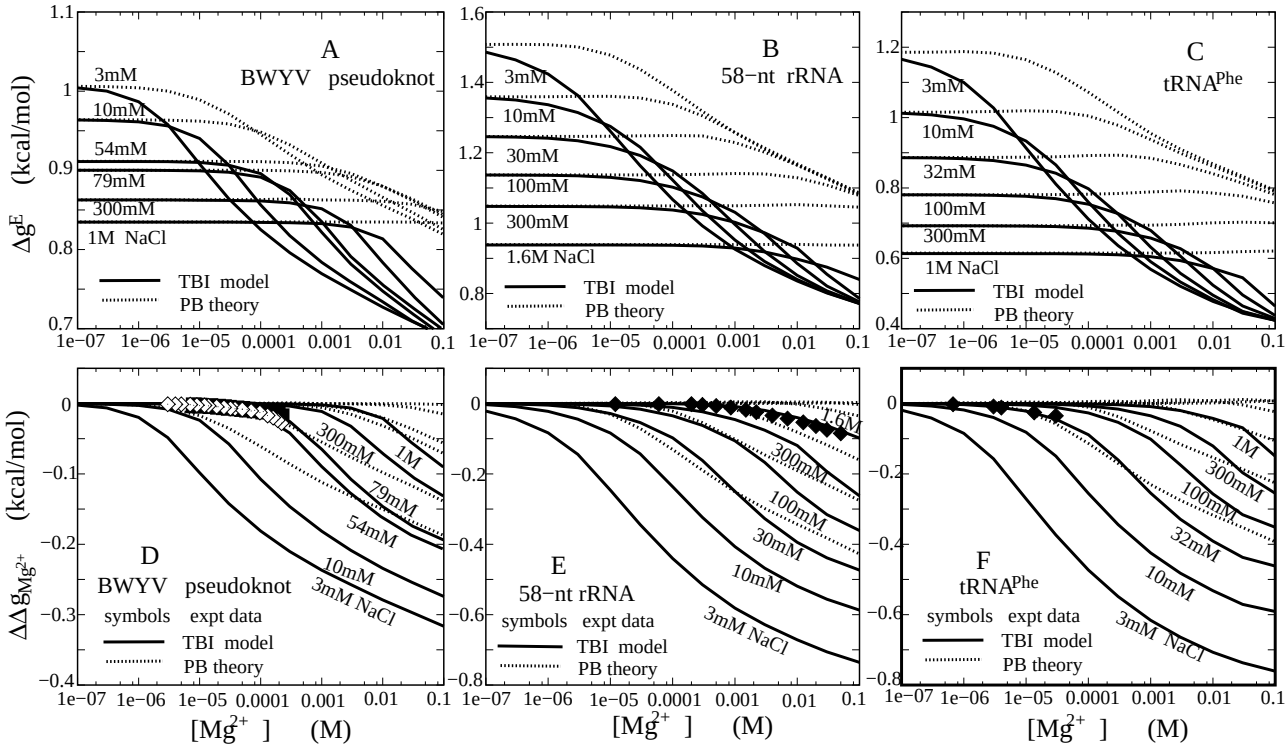

FIGURE S7 The electrostatic folding free energy $\Delta g^E=(\Delta G^E/N)$ (A-C) and Mg^{2+}-contribution $\Delta\Delta g_{Mg^{2+}}$ to tertiary structure folding free energy (D-F) for BWYV pseudoknot (A,D), 58-nt rRNA fragment (B,E), and yeast $tRNA^{Phe}$ (C,F) for mixed Na^+/Mg^{2+} solutions at room temperature. Solid lines: the TBI model; Dotted lines: the PB theory. Symbols: experimental data. (D) ◇ BWYV pseudoknot in 0.054M Na^+; ◆ BWYV pseudoknot in 0.079M Na^+ (**?**); (E) ◆ 58-nt rRNA fragment in 1.6M monovalent ion solution (18–20); (F) ◆ yeast $tRNA^{Phe}$ in 0.032M Na^+ (18, 21).

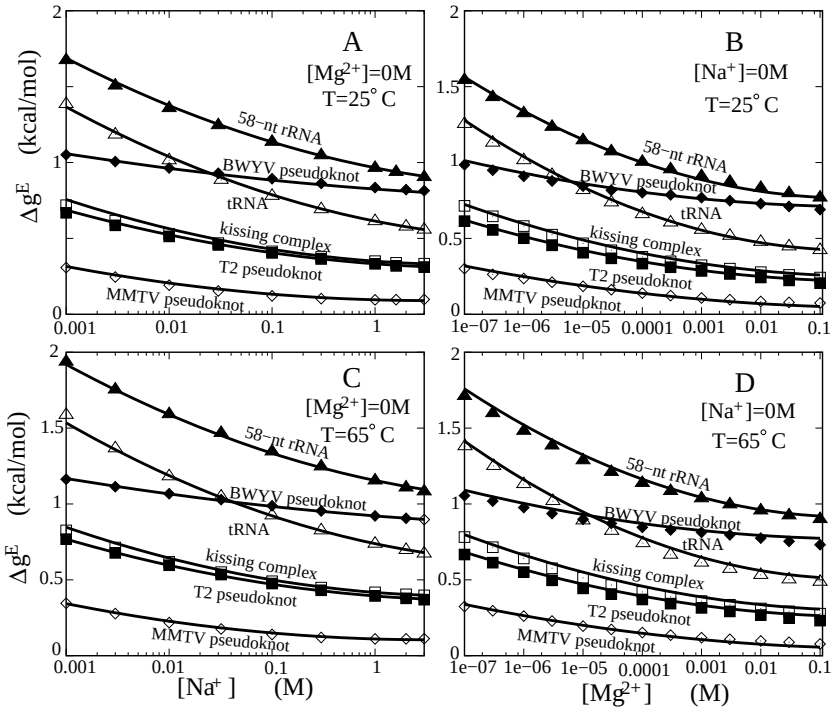

FIGURE S8 The electrostatic free energies $\Delta g^E (= \Delta G^E/N)$ for RNA tertiary folding as functions of $[Na^+]$ (A) and $[Mg^{2+}]$ (B) for six RNA molecules: BWYV pseudoknot, MMTV pseudoknot, T2 pseudoknot, kissing complex, 58-nt rRNA fragment, and yeast $tRNA^{Phe}$. Symbols: TBI model; lines: empirical formulas.

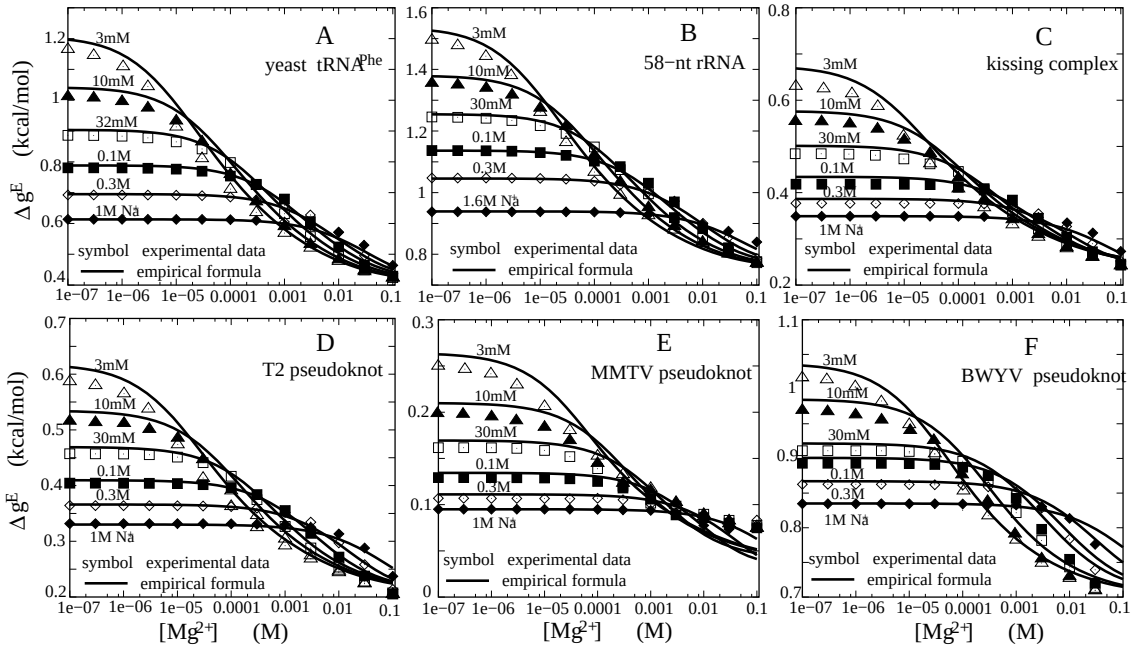

FIGURE S9 The electrostatic free energies $\Delta g^E (= \Delta G^E/N)$ for RNA tertiary folding in mixed Na^+/Mg^{2+} solutions for six RNA molecules at room temperature: yeast $tRNA^{Phe}$ (A); 58-nt rRNA fragment (B); kissing complex (C); T2 pseudoknot (D); MMTV pseudoknot (E), and BWYV pseudoknot (F). Symbols: TBI model; lines: empirical formulas.

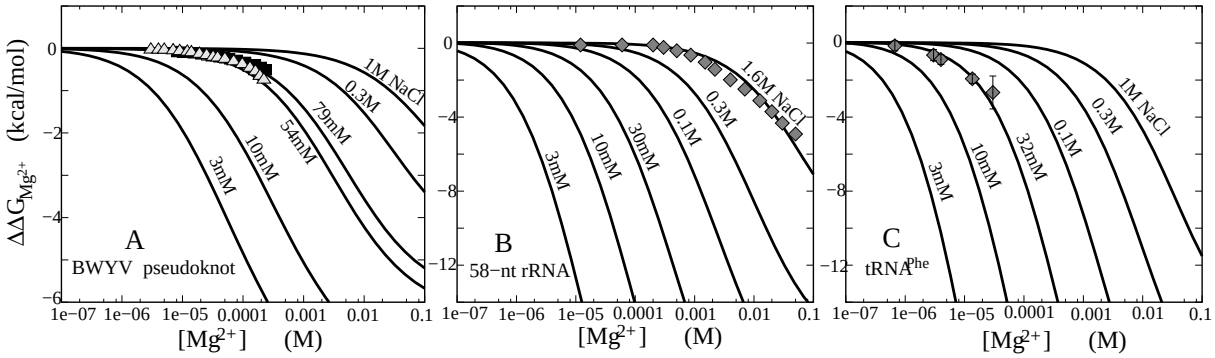

FIGURE S10 The Mg^{2+}-contribution $\Delta\Delta G_{Mg^{2+}}$ to RNA tertiary structure folding free energy as a function of $[Mg^{2+}]$ for three RNA molecules: BWYV pseudoknot (A), 58-nt ribosomal RNA fragment (B), and yeast $tRNA^{Phe}$ (C) at room temperature. Solid lines, empirical formulas derived from the TBI model; symbols, experimental data: (A) BWYV pseudoknot in 54mM and 79mM Na^+ solution (17); (B) 58-nt rRNA fragment in solution with 1.6M monovalent ions (19, 20); (C) yeast $tRNA^{Phe}$ in solution with 32mM Na^+ (19, 21).

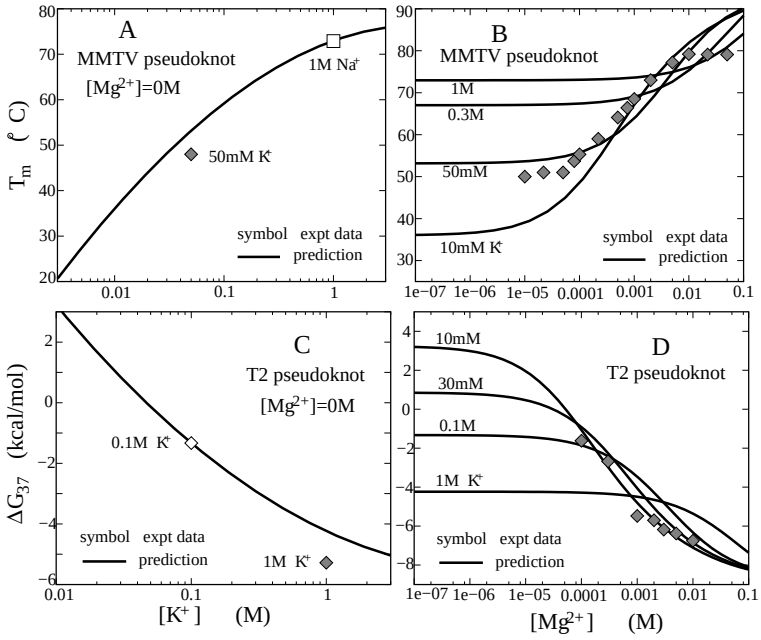

FIGURE S11 (A,B) The melting temperature T_m of MMTV pseudoknot as a function of $[K^+]$ (A) and $[Mg^{2+}]$ (B). experimental data: (A) MMTV pseudoknot in pure Na^+ or K^+ (24); (B) MMTV pseudoknot in Mg^{2+} solution with 50mM K^+ (24). (C,D) The folding free energy ΔG_{37} at 37°C of T2 pseudoknot as a function of $[K^+]$ (C) and $[Mg^{2+}]$ (D). Symbols, experimental data: (C) T2 pseudoknot in pure K^+ solution (25), and (D), T2 pseudoknot in Mg^{2+} solution with 0.1M K^+ (25). Solid lines in panel (A-D), empirical formulas derived from the TBI model.

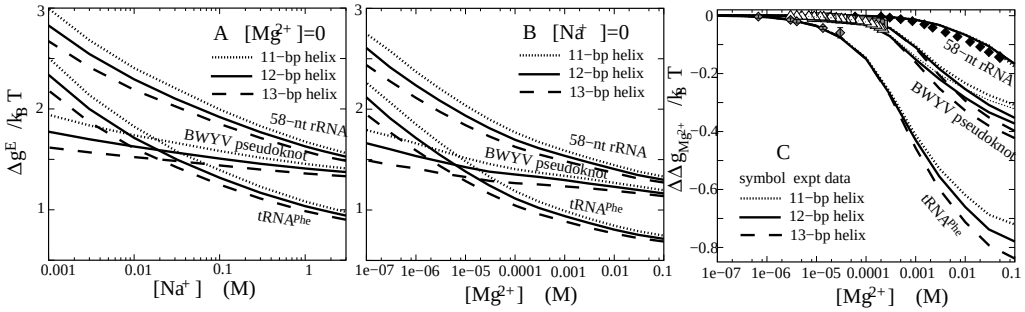

FIGURE S12 The electrostatic folding free energy Δg^E and Mg^{2+}-contribution $\Delta\Delta g_{Mg^{2+}}$ to folding free energy as functions of ion concentrations for three RNA molecules: BWYV pseudoknot, 58-nt ribosomal RNA fragment, and yeast $tRNA^{Phe}$ at room temperature. Different models of different helix length N_0 for modeling intermediate state are tested in the TBI calculations; See Methods. Lines: the TBI model with different N_0: 22-nt, 24-nt, and 26-nt. Symbols: experimental data, as shown in Fig. 2 in the main text (17, 19–21).